Intra brainstem connectivity is impaired in chronic fatigue syndrome

Leighton R Barnden[a,*], Zack Y Shan[a,b], Donald R Staines[a], Sonya Marshall-Gradisnik[a], Kevin Finegan[c], Timothy Ireland[c], Sandeep Bhuta[c]

[a] National Centre for Neuroimmunology and Emerging Diseases, Menzies Health Institute Queensland, Griffith University, Southport, QLD 4222, Australia
[b] Sunshine Coast Mind and Neuroscience Thompson Institute, University of the Sunshine Coast, Birtinya, QLD 4575, Australia
[c] Medical Imaging Department, Gold Coast University Hospital, Parklands, QLD 4215, Australia

ARTICLE INFO

ABSTRACT

In myalgic encephalomyelitis or chronic fatigue syndrome (ME/CFS), abnormal MRI correlations with symptom severity and autonomic measures have suggested impaired nerve signal conduction within the brainstem. Here we analyse fMRI correlations to directly test connectivity within and from the brainstem. Resting and task functional MRI (fMRI) were acquired for 45 ME/CFS (Fukuda criteria) and 27 healthy controls (HC). We selected limited brainstem reticular activation system (RAS) regions-of-interest (ROIs) based on previous structural MRI findings in a different ME/CFS cohort (bilateral rostral medulla and midbrain cuneiform nucleus), the dorsal Raphe nucleus, and two subcortical ROIs (hippocampus subiculum and thalamus intralaminar nucleus) reported to have rich brainstem connections. When HC and ME/CFS were analysed separately, significant correlations were detected for both groups during both rest and task, with stronger correlations during task than rest. In ME/CFS, connections were absent between medulla and midbrain nuclei, although hippocampal connections with these nuclei were enhanced. When corresponding correlations from HC and ME/CFS were compared, ME/CFS connectivity deficits were detected within the brainstem between the medulla and cuneiform nucleus and between the brainstem and hippocampus and intralaminar thalamus, but only during task. In CFS/ME, weaker connectivity between some RAS nuclei was associated with increased symptom severity. RAS neuron oscillatory signals facilitate coherence in thalamo-cortical oscillations. Brainstem RAS connectivity deficits can explain autonomic changes and diminish cortical oscillatory coherence which can impair attention, memory, cognitive function, sleep quality and muscle tone, all symptoms of ME/CFS.

1. Introduction

ME/CFS is a common, debilitating, multisystem disorder of uncertain pathogenesis, for which there exists evidence of dysregulation of the central nervous system, immune system and cellular energy metabolism (Carruthers et al., 2011).

The brainstem, which consists of the midbrain, pons and medulla, has recently been implicated in ME/CFS. Three observations in cross-sectional MRI studies have implied that nerve signal conduction through the brainstem is impaired in ME/CFS. Firstly, more severe ME/CFS was associated with increased myelination in the internal capsule (Barnden et al., 2015). This association, at first counter-intuitive, was consistent with the thalamus upregulating internal capsule myelination

to compensate for compromised ascending signals from the brainstem. Thalamic regulation of thalamo-cortical myelination is known from earlier studies (Salami et al., 2003). Secondly, MRI interaction-with-group correlations with peripheral pulse pressure detected opposite MRI regressions in ME/CFS and HC (i.e. abnormal in ME/CFS) in several brainstem RAS nuclei (Barnden et al., 2016). These nuclei determine the signals that descend to blood pressure and other autonomic effectors, but did not themselves show MRI differences. Instead it was suggested that communication between them was impaired in ME/CFS. Thirdly, a group comparison with advanced instrumentation found *decreased* myelin in the brainstem and *increased* myelin in sensorimotor white matter (WM) (Barnden et al., 2018). A novel reciprocal relationship was demonstrated between them in both HC and ME/CFS

and presumably characterises a previously unreported mechanism that maintains adequate motor signalling through the brain stem via the thalamus to the cortex. That is, the increased sensorimotor WM myelin in ME/CFS was consistent with myelin upregulation by the thalamus to compensate for impaired signal conduction through the myelin-depleted brain stem. The myelin level conclusions were made from T1 weighted spin-echo MRI on the basis that, in WM, myelin determines 90% of T1 contrast (Stüber et al., 2014).

Central motor system connectivity deficits in ME/CFS have been observed using cerebral magnetic stimulation (Hilgers et al., 1998), but this approach could not isolate the brainstem component. Our aim was to perform direct measurement of intra-brainstem connectivity to confirm the above inferences. To this end, we acquired functional MRI (fMRI) during both resting and task states for ME/CFS and HC cohorts. In the brainstem, fMRI is susceptible to high noise levels, distortion and signal dropout. To obtain adequate brainstem images we acquired sagittal sections and optimised spatial normalization for the brainstem.

For connectivity assessment, regions of interest (ROIs) were defined so correlations between their blood oxygenation level dependent (BOLD) activity time series could be computed. The primary brainstem ROIs we selected were within the reticular activation system (RAS), bilaterally both in the rostral medulla and in the cuneiform nucleus of the midbrain. Although initially chosen because of their involvement in the MRI versus pulse pressure correlations mentioned above (Barnden et al., 2016), these medulla and midbrain regions also constitute a circuit which controls arousal levels in the cortex and gait selection[8] (Garcia-Rill et al., 2016; Gatto and Goulding, 2018). Both contain excitatory glutamatergic neurons and inhibitory neurons. In addition, cuneiform nucleus neurons have been shown to exhibit gamma band frequency oscillations (Fraix et al., 2013) which may facilitate the coherence of thalamo-cortical oscillations associated with thinking and cognition[8] (Garcia-Rill et al., 2016).

We expected the interdependent medulla and midbrain RAS locations would be most active during the cognitive task, coordinating cortical arousal and blood pressure responses, and their BOLD signal correlations would be sensitive to any connectivity deficits in ME/CFS. Brainstem – hypothalamus connectivity was also of interest, but serious signal dropout near the hypothalamus precluded defining a ROI there. We also included ROIs in the RAS dorsal Raphe nucleus, culmen of the cerebellum and subcortical structures within the thalamus and hippocampus where tractography studies had detected rich connections with the brainstem (Edlow et al., 2016; Edlow et al., 2012). Thus, given the imaging limitations, we selected limited brainstem ROIs and two subcortical ROIs to test their functional connectivity differences in ME/CFS.

2. Methods

This study was approved by the Human Research Ethics Committees of the Griffith University and the Gold Coast University Hospital where scanning was performed. We scanned 27 healthy control (HC) and 45 ME/CFS subjects who met Fukuda criteria (Fukuda et al., 1994). See (Barnden et al., 2018) for more details on subject selection.

2.1. Data collection

Resting state and task functional MRI data were acquired on a 3T MRI scanner (Skyra, Siemens) with a 64 channel head-neck coil while the subject viewed a video screen through goggles. The fMRI data were acquired sagitally using a multiband echo-planar imaging (EPI) pulse sequence developed at the University of Minnesota (Auerbach et al., 2013) with 72 slices, multiband factor = 8, TR = 798 ms, TE = 30 ms, flip angle = 40°, acquisition matrix 106 × 106 and voxel size 2 × 2 × 2 mm. High resolution structural images were acquired via a Siemens T2 'SPACE' optimized 3D fast spin-echo sequence (Mugler, 2014) with TR = 3200 ms, TE = 563 ms and variable flip angle, and with voxel size 0.88 × 0.88 × 0.9 mm. This structural scan has the spin-echo advantages

of very low distortion. Immediately before each fMRI acquisition, a single band reference EPI volume (SBRef) and two spin echo EPI volumes encoded with opposite phase directions were acquired for alignment and distortion correction purposes. A total of 1100 resting state (rfMRI) volumes were acquired in 15 min while the subject was awake and viewing a fixed stationary cross to reduce the likelihood of falling asleep. Then, a total of 1100 task fMRI (tfMRI) volumes were acquired in 15 min while the subject was performing a sequence of Stroop color-word tasks (Leung et al., 2000). The Stroop task was chosen because it tested the attention and concentration difficulties frequently reported by CFS/ME patients (Ray et al., 1993). Details of its implementation here are given in (Shan et al., 2018). During both fMRI, 200 Hz physiological measures were acquired from Siemens pulse oximeter and respiratory strap sensors. All subjects completed the 36 item Short Form Health Survey (SF36) questionnaire (Ware et al., 1995).

2.2. Regions of interest (ROIs)

ROIs used for connectivity analysis are listed in Table 1 and displayed on Fig 2. ROIs were constructed for the brainstem medulla and midbrain, based on locations where abnormality in ME/CFS autonomic regressions was detected earlier in a different cohort (Barnden et al., 2016). An extended ROI over the right-hand cuneiform nucleus of the midbrain RAS was derived from the T map of the T1wSE regression with pulse pressure (Fig 2C,D in (Barnden et al., 2016)) thresholded at $T = 5.4$. This binary map was then widened medially by shifting by 1 pixel in X and performing an OR with the original. This ROI also included the smaller pedunculopontine nucleus (PPN) (Naidich et al., 2009). This right-hand ROI was then laterally mirrored to create the left-hand cuneiform nucleus ROI.

Locations identified in (Barnden et al., 2016) were also the basis for bilateral overlapping spherical rostral medulla ROIs and a spherical left hand culmen ROI. These were created using 'marsbar' (Brett et al., 2002) with radius 6 mm and centered on $(-4\ -32\ -44)$, $(4\ -32\ -44)$ and $(-8\ -44\ -24)$. The rostral medulla ROIs overlap by 1 pixel and cover the midline caudal Raphe and bilateral paragigantocellular (LPGi) RAS nuclei. The dorsal Raphe region was extracted from the Harvard Ascending Arousal Network Atlas (www.martinos.org/resources/aan-atlas), resliced to 2 mm voxel size, and dilated in 3D by 1 pixel.

Other ROIs were selected based on tractography reports of ascending brainstem fibre destinations (Edlow et al., 2016; Edlow et al., 2012). Left and right hippocampus subiculum ROIs were extracted from the Juelich Histological Atlas distributed with the FMRIB software library (www.fmrib.ox.ac.uk/fsl), and left and right thalamus intralaminar nucleus ROIs from (Morel, 2007).

2.3. Image analysis and ROI-based functional connectivity analysis

For both rfMRI and tfMRI data:

Motion correction was applied by registering the 1100 EPI volumes to the single band reference (SBref) EPI image using MCFLIRT (Jenkinson et al., 2002) implemented in FSL. Distortion correction was applied using the distortion field calculated from the two oppositely phase-encoded spin echo EPI volumes using the "topup" toolbox (Andersson et al., 2003) as implemented in FSL (FMRIB's Software Library, www.fmrib.ox.ac.uk/fsl).

Table 1
ROIs between which connectivity was assessed. L is Left, R is Right.

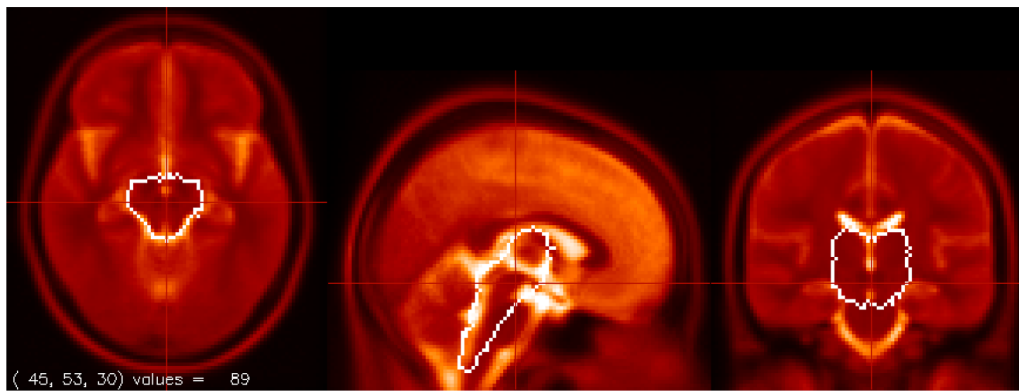| ROI location	laterality	abbreviation	Voxels
Rostral medulla	L&R	Mdul_L, Mdul_R	123
Cuneiform nucleus / PPN	L&R	CnF_L, CnF_R	125
Dorsal Raphe nucleus	midline	DoRph	129
Culmen of cerebellum	L	Culm_L	123
Subiculum of hippocampus	L&R	hippo_L, hippo_R	377
Intralaminar nucleus of thalamus	L&R	iLam_L, iLam_R	32

Fig. 1. The Brainstem + Diencephalon mask used to optimise brainstem spatial normalization shown on the T2 template. The mask excludes the ventral medulla and pons where serious signal dropout and distortion was seen in some fMRI images.

The 1100 EPI images were then spatially normalised to Montreal Neurological Institute (MNI) space using FSL's FLIRT (Jenkinson et al., 2002) in two steps to optimise brainstem registration. Firstly, the fMRI companion SBref image was deformed to the MNI T2 template with 9 degrees of freedom (DF) and with angular rotations about the X, Y and Z axes constrained to 20° Angular constraints prevented grossly inaccurate deformations in a few subjects. This 9DF deformation adjusted brain size differences. Secondly, a mask was created to isolate the brain stem and diencephalon – see Fig 1. This mask excluded the ventral half of the pons and medulla where signal dropout was observed in many subjects. The deformed image from the first step was then further deformed with 6 degrees of freedom constrained by this thalamus-brainstem mask and with the same 20° angular constraints. The two deformations were then merged and applied to the 1100 EPI images.

Each subject's structural scan was segmented into gray matter, white matter and CSF partitions which were then deformed to MNI space. BOLD time series were extracted for white matter (WM) and CSF ROIs and a principal component decomposition performed to yield WM(4 components) and CSF(10) to implement 'CompCor' (Behzadi et al., 2007) removal of noise components below. This method can effectively correct noise from motion (Behzadi et al., 2007).

Regressors for the isolation of physiological noise were computed from the companion pulsatile (pulse oximeter) and respiratory strap signals. Matlab programs were written to extract the two 200 Hz time series from the Siemens log files, compute their frequency spectra with Matlab's FFT, set values for frequencies > 3x the primary peak to zero, and generate low-noise time series with the inverse FFT. Peaks in the pulse oximeter signal were identified after outlier removal. The clean cardiac and respiratory time series were themselves used as physiological regressors and, together with the pulse oximeter peak locations were processed with the PhysIO program (Kasper et al., 2017) to generate another 15 RETROICOR (Hu et al., 1995) physiological regressors for denoising.

Denoised BOLD time series were then generated from the registered EPI images from 2.3.3 using the CONN package (Whitfield-Gabrieli and Nieto-Castanon, 2012) as follows:

(a) Discard the first 5 of 1100 fMRI EPI volumes to ensure that tissue magnetization had reached steady state.
(b) Smooth with a 3 mm full width at half maximum Gaussian kernel.
(c) Compute raw BOLD ROI time series from the mean signal in the volumes of (b).
(d) Apply a general linear model to isolate the 'CompCor' and 'RetroIcor' noise signals from the EPI series of (c).

Note that no spatial normalization was performed within CONN.

CONN second-level analysis tested for connectivity between pairs of ROI locations using the Z-scores from Fisher's transformed Pearson correlation coefficient for each subject. Initially we tested for connectivity in the ME/CFS and HC groups separately, and then for connectivity differences between them. For each test we assessed the T statistic and p value corrected for false discovery rate (p-FDR). Comparison between ME/CFS and HC of the number of connections with p-FDR < 0.05 was confounded by the different number of subjects N (44 vs 26 for task), so the CFS task test was repeated with the same N as the HC (first 9 and last 9 subjects acquired were omitted). All tests included adjustment for age and gender.

Associations between connectivity and symptom severity were evaluated using regressions of the inter-ROI correlation Z for each subject in the ME/CFS group against their ME/CFS severity scores. Severity measures included the SF36 physical and mental summary scores and 3 Stroop test scores (reaction time, accuracy and Stroop effect). Significant CFS regressions were extended to also test for a difference from the corresponding HC regression in interaction-with-group analyses.

3. Results

Visual inspection found unacceptable signal dropout or inadequate spatial normalization in the resting fMRI in 3 ME/CFS and 2 HC, and in the task fMRI in one ME/CFS and one HC. These subjects were excluded from the analysis.

3.1. Connectivity in separate groups

We first examined connections in the HC and ME/CFS groups separately. To our knowledge this is the first fMRI connectivity study of these brainstem nuclei.

Table 2 lists the group T statistic for the test that correlation Z differed from zero for 33 of the 45 possible connections between the 10 ROIs. If a ROI pair for either HC or ME/CFS correlated with p-FDR < 0.05, T for both groups are shown. The remaining 12/45 ROI pairs showed no correlation in either group for either rest or task. Notable for their absence in ME/CFS, for both rest and task, were correlations, between the medulla and CnF and, for rest, between the medulla and DoRph. For both HC and ME/CFS for rest and task, the overlapping Mdul_L and Mdul_R in the rostral medulla were very strongly correlated as were the well separated hippo_L and hippo_R of the bilateral hippocampus subiculum. Both hippocampus regions correlated strongly with the right cuneiform nucleus in ME/CFS. During the task 24 ME/CFS and 23 HC connections were significant, although the ME/CFS count fell to 18 after repeating its analysis with the same N = 26 as HC. For the rest analysis, 18 ME/CFS and 15 HC connections were significant, and the ME/CFS count was 16 with the same N as HC (data not shown).

In the task fMRI for the same 10 ROIs (Fig 3 lower panels) there were more correlations than for the rest fMRI for both HC and ME/CFS.

Table 2
For rest and task fMRI, for HC and CFS groups, the group T statistic for the test that Z for each pair of ROIs differed from zero. T are listed for 33/45 pairs from 10 ROIs. All other pairs were insignificant. T are shown for both groups when, for either group, correlation p-FDR < 0.05. The bottom row is the number of significant connections for each group.

ROI 1	ROI 2	rest HC	CFS	Task HC	CFS	CFS
N		24	39	26	44	26
Mdul_L	Mdul_R	10.2	14	18	17	13
	CnF_L			3.8*	−1.1†	
	DoRph			0.4†	2.3	1.8†
	Culm_L			2.4	3.3	2.5
	hippo_L	2.3	2.9	3.6	3.0	2.7
	hippo_R	2.4	4.1	1.6†	4.0	4.0
Mdul_R	CnF_L			4.3*	−0.6†	
	Culm_L			2.6	2.7	2.1†
	hippo_L			4.7*	2.0†	1.4†
	hippo_R	1.6†	3.9	2.4	3.1	1.8†
CnF_L	CnF_R	1.6†	4.8	2.2	3.5	3.1
	DoRph	2.1	4.9	3.5	4.1	3.5
	Culm_L	3.3	1.8†			
	hippo_L	3.4	3.9	4.0	4.3	3.0
	hippo_R			2.5	2.2	2.1
	iLam_L	1.3†	2.5			
CnF_R	DoRph	3.4	4.0	4.0	4.8	4.2
	Culm_L			2.5	1.5†	
	hippo_L	3.2	4.3	1.4†	4.7	3.3
	hippo_R	2.2	3.5	0.9†	4.3	3.2
	iLam_R			2.4	0.2†	
DoRph	Culm_L	3.5	3.1	2.2	3.8	4.1
	hippo_L	0.9†	3.1	2.7	3.1	2.3
	hippo_R	2.4	4.3	2.1	4.5	3.4
	iLam_L	1.6†	2.5	2.6	0.6†	
	iLam_R			3.2*	0.2†	0.02†
Culm_L	hippo_L	3.9	3.9	4.5	2.9	1.1†
	hippo_R	1.5†	3.2	2.2†	3.7	2.6
hippo_L	hippo_R	6.1	11.2	7.0	9.4	6.7
	iLam_L			0.9†	3.1	2.4
	iLam_R	2.7	1.3†			
hippo_R	iLam_L			1.9†	2.1	1.8†
iLam_L	iLam_R	3.5	2.7†	1.0†	3.7	3.7
significant connections		15	18	24	23	18

*flags correlations with significantly impaired CFS connectivity (Table 3).,
†flags insignificant group correlation.

3.2. Connectivity differences between groups

We then tested for differences in connectivity between HC and ME/CFS. For the resting fMRI, no connectivity differences between the groups were found for any of the ROI pairs. For the task fMRI, four pairs of ROIs were found to demonstrate reduced connectivity in ME/CFS as seen in Fig 4 and Table 3. Two pairs were within the brainstem from the rostral medulla to the midbrain CnF and two were between the brainstem and the two subcortical centres tested.

3.3. Associations between connectivity and ME/CFS severity

Regressions of individual subject brainstem connectivity with ME/CFS severity yielded 3 significant associations for the ME/CFS group during task fMRI but none for rest. Table 4 (1 s column) shows associations for Mdul_L to hippo_R connectivity with the SF36 physical summary score, and for hippo_L to iLam_R and hippo_L to Culm_L connectivity with the SF36 mental summary score. The 2 s column shows a significant mentSF36 interaction-with-group regression (opposite regression slopes for HC and ME/CFS) for the hippo_L to Culm_L correlation. The isolated HC regression was not significant. Group values for the SF36 and Stroop measures regressed here can be found in (Shan et al., 2018).

Table 3
For the task fMRI, the T and *p*–FDR (false discovery rate corrected) statistics for HC connectivity greater than ME/CFS connectivity for ROI pairs within the brainstem (top 2 rows) and between ROIs in the brainstem and two subcortical ROIs. See Table 1 for abbreviations.

ROI 1	ROI 2	T	p-FDR
Mdul_R	CnF_L	4.2	.0009
Mdul_L	CnF_L	3.6	.003
Mdul_R	hippo_L	3.2	.01
DoRph	iLam_R	3.0	.03

Table 4
Significant (p-FDR < 0.05) regressions between CFS brainstem connectivity during task vs CFS severity regressor. The 1 s column lists the single group (CFS) regressions and 2 s shows the one interaction-with-group (opposite CFS and HC regression) significant result. Regressors physSF36 and mentSF36 refer to the SF36 physical and SF36 mental summary scores.

ROI 1	ROI 2	regressor	1s	2s
hippo_R	Mdul_L	physSF36	0.040	
hippo_L	Culm_L	mentSF36	0.034	
hippo_L	iLam_R	mentSF36	0.038	

4. Discussion

The primary aim was fulfilled and deficits in intra-brainstem connectivity in ME/CFS relative to HC were demonstrated between the medulla and the midbrain, but only during the cognitive task. Connectivity between the brainstem and two subcortical nuclei was also reduced in ME/CFS.

Connectivity within the separate HC and ME/CFS groups, and associations of this connectivity with severity in ME/CFS was also detected. We believe this is the first report of connectivity for these brainstem nuclei.

4.1. Regions of interest

Implicit in our choice of ROIs to investigate brainstem connectivity is the assumption that the large white matter tracts that traverse the brainstem do not exhibit a BOLD response to neuronal activity. Rather, BOLD responses are associated with the neurons distributed through the nuclei of the reticular activation system (RAS). Because of spatial resolution and spatial normalization limitations we avoided very small RAS nuclei. The RAS bilateral medulla and cuneiform nucleus ROIs were chosen on the basis of their previously reported involvement with ME/CFS (Barnden et al., 2016). Their locations in the medulla and midbrain are spatially well separated (Fig 2, $x = -8$) and contain relatively large RAS nuclei (Naidich et al., 2009). The lateral paragigantocellular (LPGi) nucleus in the medulla ROIs and the cuneiform nucleus and PPG in the CnF ROIs have important reciprocal connections (Gatto and Goulding, 2018) and so were ideal for testing for connectivity differences in ME/CFS. The thalamus intralaminar nucleus ROIs were chosen because of their rich connections to the cuneiform nucleus (Edlow et al., 2012), and their component parafascicular nucleus is regarded as an integral part of the RAS (Garcia-Rill et al., 2013). The midbrain Dorsal Raphe and hippocampus subiculum ROIs were chosen because of their interconnections (Edlow et al., 2016) and both have a relatively large size. The left culmen ROI had also been involved with ME/CFS (Barnden et al., 2016) and covers parts of the deep cerebellar nuclei.

4.2. Connectivity in separate groups

When analysed separately, both the HC and ME/CFS groups demonstrated strong fMRI correlations (Table 2, Fig 3) between the brainstem and the two subcortical nuclei tested, and within the
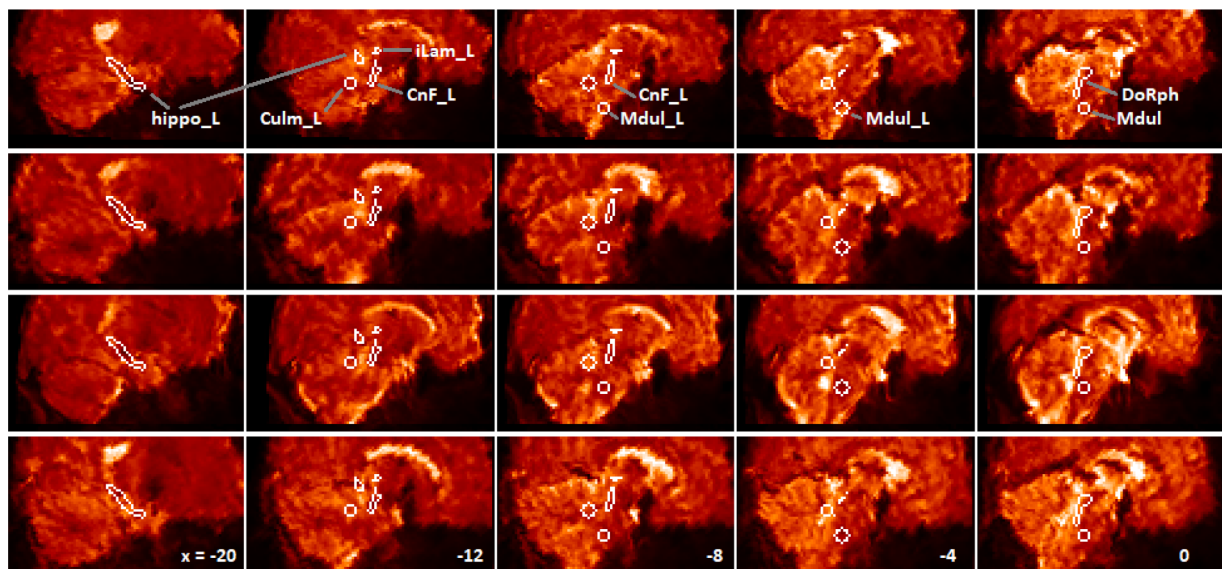
Fig. 2. Para-midline sagittal sections, after optimised spatial normalization, of the fMRI mean image of 4 subjects (one per row) to illustrate noise and variable signal dropout. Columns from left are for $x = -20, -12, -8, -4, 0$ mm relative to midline. One of each bilateral ROI (left side) and the midline dorsal Raphe ROI are labelled in the top row (hippo: hippocampus subiculum, Culm: culmen, CnF: cuneiform nucleus, Mdul: rostral medulla, iLam: thalamus intralaminar nucleus, DoRph: dorsal Raphe nucleus). The edge voxels are within the ROI. Note on the midline at right, the variable distortion / signal loss on the ventral surface of the brainstem while the dorsal surface is relatively well-preserved. Note also signal dropout near the hypothalamus.

brainstem for HC. In ME/CFS the loss of Mdul - CnF connections was associated with multiple enhanced hippocampal connections to the medulla and CnF (Table 3), suggesting the hippocampus may have a compensatory function, but no enhancement was significant (hippo_L – CnF_R was strongest with p-FDR = 0.17). As expected, correlations were more extensive during the cognitive task (more network connections were activated) when RAS nuclei would be actively coordinating cortical arousal and hemodynamic responses. The strong correlations between the left and right medulla are expected because there is partial overlap at the midline, which could indicate strong BOLD involvement of the midline median Raphe nucleus and/or correlated BOLD responses for the lateral paragigantocellular nuclei (LPGi) on each side. The strong correlations between the bilateral hippocampal ROIs presumably also indicate strong connectivity and parallel functions. Comparing the number of connections in the CFS/ME group relative to HC is confounded by the larger cohort for CFS/ME (44 versus 26 for task). When the same number of ME/CFS subjects as HC were analysed during task there were actually fewer significant connections than for HC.

4.3. Regressions between RAS connectivity and ME/CFS severity

Table 4 shows that the strength of three brainstem connections in CFS/ME during task was associated with symptom severity. This provides support for the notion that impaired brainstem connectivity is an important factor in CFS/ME aetiology. One node of each of these connections was in the hippocampus. Detection of a significant interaction-with-group regression for hippo_L to Culm_L connectivity versus the SF36 mental summary score determines that this association was abnormal in CFS/ME. The variance introduced by this association with physical and mental wellbeing can degrade the group statistics for the connections involved (Table 4) and may account for insignificance of hippo_L vs iLam_R in Table 2.

4.4. Functional connectivity deficits in ME/CFS

The strongest ME/CFS deficits were seen for connectivity between the medulla (both left and right) and the *left* cuneiform nucleus. It was the contralateral *right* cuneiform nucleus, however, that was involved with abnormal blood pressure correlations (Barnden et al., 2016). The

cause of connectivity deficits in the brain stem needs to be further investigated. Perturbations in calcium metabolism have been reported in ME/CFS (Nguyen et al., 2017). The role of Ca^{2+} in relevant astrocyte support and/or oscillatory performance of RAS neurons is yet to be established. It is also worth noting that neuroinflammation has been observed in ME/CFS (Nakatomi et al., 2014) and that the brainstem is particularly sensitive to hypoxia (Marina et al., 2015). While the consequences of RAS connectivity deficits in such a complex system are difficult to predict, they can be expected to influence initiation and maintenance of movement, sleep quality, autonomic function and cortical arousal levels which affect memory, learning and problem solving, and therefore contribute to many of the symptoms of ME/CFS.

Brainstem – subcortical connections between the DoRph and intralaminar nucleus of the thalamus, and between the rostral medulla and hippocampus were also impaired in ME/CFS. The former suggests that the phenomenon that affects intra-brainstem medulla-to-midbrain connectivity extends at least to the medial midbrain to affect ascending dorsal Raphe projections.

4.5. Reticular activation system

RAS neurons influence cortical function via two different processes. Firstly RAS neuron projections deliver neurotransmitters directly or indirectly (via hypothalamus, basal forebrain) to the cortex (Saper and Fuller, 2017), and secondly RAS neurons generate oscillatory electrical signals that facilitate the coherence of *cortical* oscillations necessary for attention, sensory perception, problem solving and memory (Garcia-Rill et al., 2013). RAS nuclei connect with each other and to the body and subcortical and cortical structures. Elevated cortical or physical activity feeds back to the RAS to further raise cortical arousal levels. The RAS ROIs examined here included the midbrain cuneiform nucleus and PPN which contain excitatory glutamatergic and cholinergic neurons and some inhibitory neurons, and the rostral medulla where the LPGi also contains glutamatergic and inhibitory nuclei. Together they constitute a circuit that controls both cortical arousal levels (cognition / wake / sleep) and gait selection (eg walking or running) (Gatto and Goulding, 2018) in response to inputs from multiple brain centres. Inhibitory neurons in the LPGi influence the cuneiform nucleus to reduce cortical activity or initiate sleep.
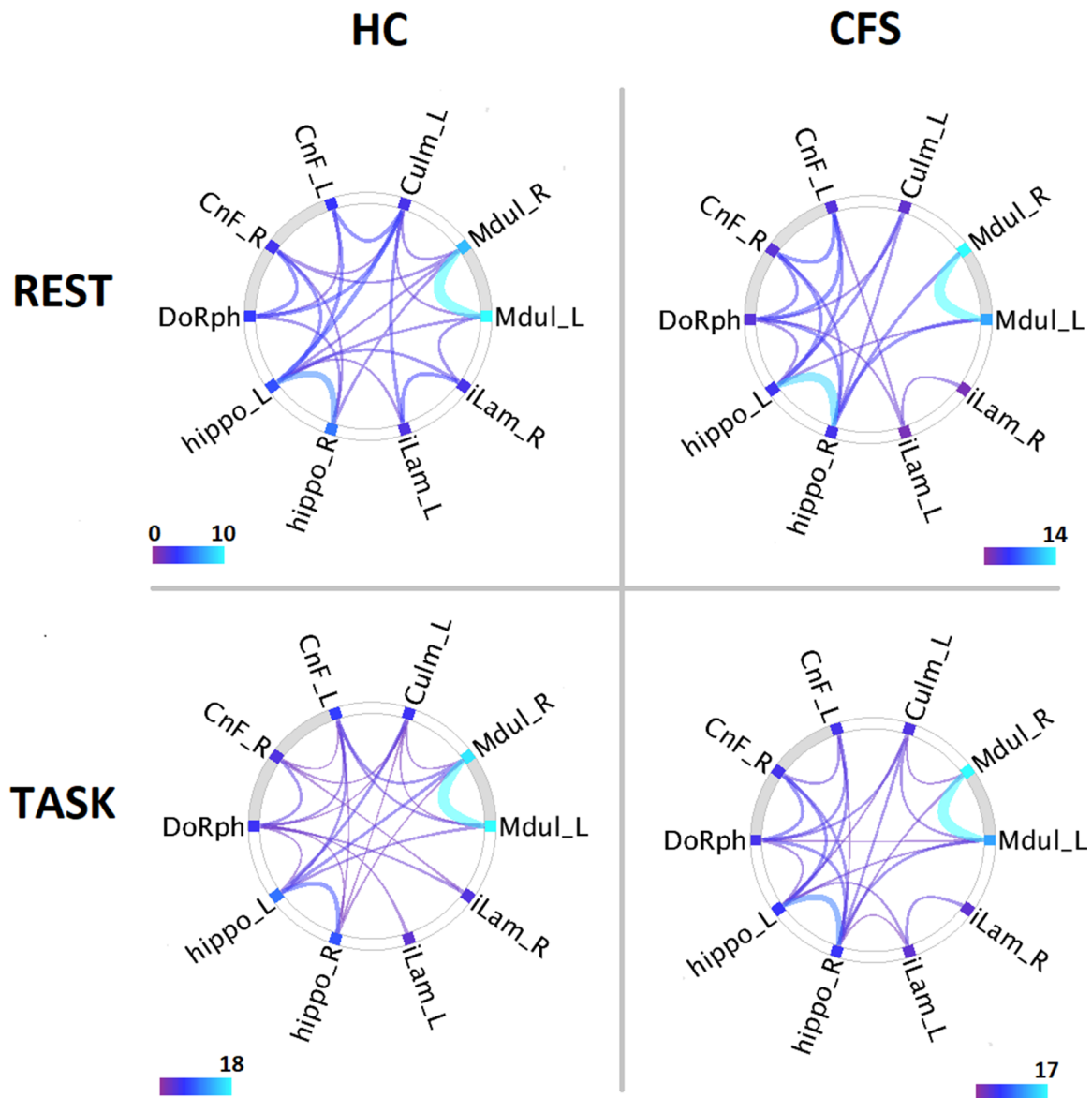
Fig. 3. Connectogram summary of significant connectivity for the healthy control (HC) and ME/chronic fatigue syndrome (CFS) groups during Rest and Task fMRI. All correlations were positive. In CFS there were no Mdul - CnF connections. Connectivity for joined ROIs was significant with p_FDR < 0.05. Line width and color encode the T statistic for non-zero group connectivity. The grey arcs highlight the brainstem midbrain (left) and medulla (right) nodes.

It is now known that RAS neurons can fire repeatedly generating oscillatory signals. The cuneiform nucleus and PPN fire at the high frequencies of the gamma band. Gamma band oscillations also occur in the thalamus and cortex (Garcia-Rill et al., 2013). RAS nuclei contain neuron subpopulations with electrical (gap junction) synapses that facilitate synchronous gamma band oscillation (Garcia-Rill et al., 2013; Garcia-Rill et al., 2016). An important property of gamma band oscillations is coherence which describes the synchrony between oscillations in spatially separated structures. During cognitive processing, gamma band oscillations in both the RAS cuneiform nucleus / PPN and thalamic intralaminar (parafascicular) neurons are believed to facilitate and stabilize the coherence of *cortical* oscillations (Garcia-Rill et al., 2013; Garcia-Rill et al., 2016) which is important for attention, sensory perception, memory and problem solving (Garcia-Rill et al., 2013).

4.6. Physiological artifacts

Pulsatile and/or respiratory effects that influence fMRI signals from any pair of ROIs can result in a strong correlation between their time series that is not neurological in origin and therefore yields erroneous

conclusions about their connectivity. Such physiological modulation will be more severe in the brainstem with its proximity to major cerebral arteries. To isolate artifactual temporal components from the fMRI time series here, in addition to the CompCor covariates (see Methods) we included extensive physiological covariates derived from companion pulsatile and respiratory measurements. Although there remains a concern that some non-neurological component may persist, successful artifact removal is indicated because 'seed to voxel' analysis (not shown) did not show extended areas of correlation for any of the brainstem seeds (ROIs), and correlations were absent between many brainstem ROIs (e.g. Mdul_L and CnF_R). Of importance to the main finding here is, when comparing connectivity of the HC and ME/CFS groups, a systematic artifactual component is unlikely to induce a difference between them. The discussion here assumed physiological artifacts were effectively removed.

4.7. Limitations

As with most cross-sectional studies, differences detected at the group level do not translate into 'biomarkers' useful for identifying the disease in individual subjects. Identification of the RAS as an important player in
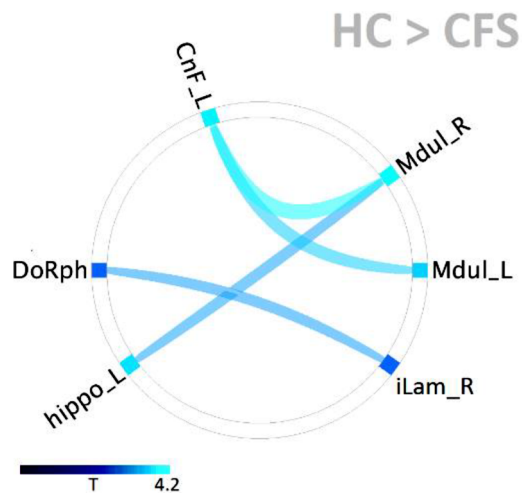
Fig. 4. Distribution of ME/CFS functional connectivity deficits relative to HC. All were significant with p-FDR < 0.05. Two pairs of ROIs (Mdul_L to CnF_L and Mdul_R to CnF_L) were located within the brainstem and showed the strongest deficits (Table 3). The other two pairs had one ROI within the brainstem. See Table 1 for abbreviations.

ME/CFS symptomatology may however open new diagnostic options (Garcia-Rill et al., 2016). The high noise levels and signal dropout associated here with the short TR (0.798 s) fMRI pose a challenge to assessment small structures in the brainstem RAS and precluded use of hypothalamus regions here. The higher frequencies detected in the BOLD response may partly offset this. Imposing a limited high frequency response by applying a [0.008 0.3] Hz band-pass filter to the BOLD responses rendered the Mdul_L to hippo_L connectivity deficit in Table 3 insignificant, although the other three deficits were slightly stronger. The use of spin echo, as distinct from gradient echo, fMRI sequences can avoid problems of signal dropout but not noise, and the longer TR involved may reduce the sensitivity to connectivity changes.

5. Conclusions

In ME/CFS, connectivity is impaired within the brainstem RAS and from the brainstem to key subcortical structures. This may explain many of the symptoms of ME/CFS. In ME/CFS, multiple hippocampal connections to the midbrain cuneiform nucleus and the medulla are enhanced, suggesting the hippocampus has a compensatory role for the impaired connections.

Acknowledgements

References

Carruthers, B., et al., 2011. Myalgic encephalomyelitis: international consensus criteria. J Intern Med 270, 327–338.

Barnden, L., et al., 2015. Evidence in chronic fatigue syndrome for severity-dependent upregulation of prefrontal myelination that is independent of anxiety and depression. NMR Biomed 28 (3), 404–413.

Salami, M., et al., 2003. Change of conduction velocity by regional myelination yields constant latency irrespective of distance between thalamus and cortex. Proc Nat Accad Sci 100, 6174–6179.

Barnden, L., et al., 2016. Autonomic correlations with mri are abnormal in the brainstem vasomotor centre in chronic fatigue syndrome. NeuroImage: Clinical 11, 530–537.

Barnden, L.R., et al., 2018. Hyperintense sensorimotor T1 spin echo mri is associated with brainstem abnormality in chronic fatigue syndrome. Neuroimage Clin 20, 102–109.

Stüber, C., et al., 2014. Myelin and iron concentration in the humanbrain:a quantitative study of mri contrast. Neuroimage 93, 95–106.

Hilgers, A., Frank, J., Bolte, P., 1998. Prolongation of central motor conduction time in chronic fatigue syndrome. J Chronic Fatigue Synd 4 (2), 23–32.

Garcia-Rill, E., et al., 2013. Coherence and frequency in the reticular activating system (RAS). Sleep Med Rev 17 (3), 227–238.

Garcia-Rill, E., et al., 2016. Arousal and the control of perception and movement. Curr Trends Neurol 10, 53–64.

Gatto, G., Goulding, M., 2018. Locomotion control: brainstem circuits satisfy the need for speed. Current Biology 28 (6), R256–R259.

Fraix, V., et al., 2013. Pedunculopontine nucleus area oscillations during stance, stepping and freezing in parkinson's disease. PLoS ONE 8 (12) e83919-e83919.

Edlow, B., et al., 2016. The structural connectome of the human central homeostatic network. Brain Connect 6 (3), 187–200.

Edlow, B., et al., 2012. Neuroanatomic connectivity of the human ascending arousal system critical to consciousness and its disorders. J Neuropath Exp Neurol 71 (6), 531–546.

Fukuda, K., et al., 1994. The chronic fatigue syndrome: a comprehensive approach to its definition and study. Ann Intern Med 121, 953–959.

Auerbach, E.J., et al., 2013. Multiband accelerated spin-echo echo planar imaging with reduced peak rf power using time-shifted rf pulses. Magn Reson Med 69 (5), 1261–1267.

Mugler, J.P., 2014. 3rd, Optimized three-dimensional fast-spin-echo mrI. J Magn Reson Imaging 39 (4), 745–767.

Leung, H.C., et al., 2000. An event-related functional mri study of the stroop color word interference task. Cereb Cortex 10 (6), 552–560.

Ray, C., Phillips, L., Weir, W.R., 1993. Quality of attention in chronic fatigue syndrome: subjective reports of everyday attention and cognitive difficulty, and performance on tasks of focused attention. Br J Clin Psychol 32 (Pt 3), 357–364.

Shan, Z.Y., et al., 2018. Brain function characteristics of chronic fatigue syndrome: a task fMRI study. Neuroimage Clin 19, 279–286.

Ware Jr., J.E., et al., 1995. Comparison of methods for the scoring and statistical analysis of SF-36 health profile and summary measures: summary of results from the medical outcomes study. Med Care 33 (4 Suppl), As264–As279.

Naidich, T., et al., 2009. Duvernoy's Atlas of the Brainstem and cerebellum. High-Field MRI: Surface anatomy, Internal structure, Vascularisation and 3D Anatomy. SpringerWienNewYork.

Brett, M., et al., 2002. Region of interest analysis using an spm toolbox [abstract]. In: Proc 8th International Conference on Functional Mapping of the Human Brain.

Morel, A., 2007. Stereotactic Atlas of the Human Thalamus and Basal Ganglia. Informa Healthcare, New York London.

Andersson, J.L., Skare, S., Ashburner, J., 2003. How to correct susceptibility distortions in spin-echo echo-planar images: application to diffusion tensor imaging. Neuroimage 20 (2), 870–888.

Jenkinson, M., et al., 2002. Improved optimization for the robust and accurate linear registration and motion correction of brain images. Neuroimage 17 (2), 825–841.

Behzadi, Y., et al., 2007. A component based noise correction method (CompCor) for bold and perfusion based fMRI. Neuroimage 37 (1), 90–101.

Kasper, L., et al., 2017. The physio toolbox for modeling physiological noise in fMRI data. J Neurosci Methods 276, 56–72.

Hu, X., et al., 1995. Retrospective estimation and correction of physiological fluctuation in functional mri. Magn Reson Med 34 (2), 201–212.

Whitfield-Gabrieli, S., Nieto-Castanon, A., 2012. Conn: a functional connectivity toolbox for correlated and anticorrelated brain networks. Brain Connect 2 (3), 125–141.

Nguyen, T., et al., 2017. Impaired calcium mobilization in natural killer cells from chronic fatigue syndrome/myalgic encephalomyelitis patients is associated with transient receptor potential melastatin 3 ion channels. Clin Exp Immunol 187 (2), 284–293.

Nakatomi, Y., et al., 2014. Neuroinflammation in patients with chronic fatigue syndrome/myalgic encephalomyelitis: an 11C-(R)-PK11195 PET study. J Nucl Med 55, 945–950.

Marina, N., et al., 2015. Brainstem hypoxia contributes to the development of hypertension in the spontaneously hypertensive rat. Hypertension (Dallas, Tex.: 1979) 65 (4), 775–783.

Saper, C.B., Fuller, P.M., 2017. Wake-sleep circuitry: an overview. Curr. Opin. Neurobiol. 44, 186–192.